Performance of loop thermosyphon solar water heater with four evaporators and U-symmetric heads

Chien Huang [a], Wei-Keng Lin[a], Sung-Ren Wang [a] and Shao-Wen Chen [a]

[a] Engineering & System Science Department National Tsing-Hua University, Hsinchu, Taiwan,
wklin@ess.nthu.edu.tw

Abstract:

In this paper, we report experimental results for two different designs of U-symmetric heads loop thermosyphon devices with four evaporators to be used as solar collectors, as shown in Fig. 1. Experiments were conducted to investigate thermal storage efficiency and temperature distributions in the devices at different values of input power and different lengths of the porous wick. We find that the length of the porous wick had a critical impact on thermal storage efficiency, especially at low input power. The best thermal storage efficiency was 80%, which is higher than that of a conventional flat-plate solar water heater. In addition, the U-symmetric heads led to nearly uniform temperature distributions in each of the four evaporators.

Keywords:

Solar water heater; Thermal storage efficiency; Loop thermosyphon; Multiple evaporators

1. Introduction

A loop thermosyphon is a high-efficiency heat transfer device that uses the phase change of a working fluid to transfer heat from an evaporator to a condenser. In such a device, the vapor and liquid flows are separated and gravity is used to drive the condensed working fluid back to the evaporator, as shown in Fig. 1. As a result, a loop thermosyphon has a low pressure drop and can transport heat over long distances. A loop thermosyphon offers many advantages when applied in solar water heating [1, 2]: (a) low heat capacity, (b) no mechanical pumping is needed to circulate the working fluid, (c) simple protection against freezing, and (d) when the evaporator temperature is less than the temperature of the stored water, heat does not flow back to the evaporator.

Over the last few years, loop thermosyphon solar water heaters have been widely investigated. Chien et al. performed theoretical and experimental studies of a two-phase thermosyphon solar water heater. They found the best charge efficiency of the system to be 82%, which is higher than that of a conventional solar water heater [3]. Lu et al. investigated the thermal performance of an open thermosyphon using nanofluids in high-temperature evacuated tubular solar collectors. Their system used deionized water and water-based CuO nanofluids as the working liquid. They found that the mass concentration of CuO nanoparticles had a remarkable influence on the heat transfer coefficient in the evaporator, and that a mass concentration of 1.2% provided the optimal enhancement of heat transfer [4]. Zhang et al. investigated a solar photovoltaic/loop-heat-pipe heat pump system for heating water. Under their experimental conditions, the overall efficiencies of the PV/LHP module were around 50%, while the overall performance coefficient of the system was 8.7 [5, 6]. Li et al. introduced an insert-type closed-loop thermosyphon for split-type solar water heaters [7]. Their experimental results indicated that by using the proposed thermosyphon, the water heater provided twice the heating speed compared to that with a conventional thermosyphon.

These examples illustrate that the loop thermosyphon is suitable for use as a solar water heater. However, to our knowledge, the temperature distributions in the each evaporators have not been investigated. And the U-symmetric heads led to nearly uniform temperature distributions in each of the four evaporators. In this study, two different loop thermosyphon collectors were designed and tested, as shown in Fig. 2. Our main objectives were to study temperature distributions in each evaporator, evaluate the thermal storage efficiency, determine the effects of the porous wick, and investigate sharing of heat load for two designs of loop thermosyphon collectors under different values of input power.

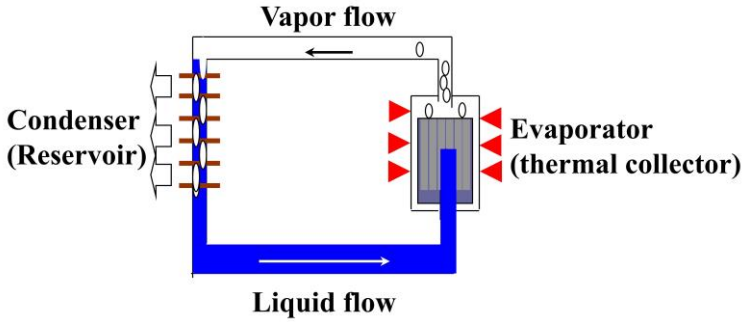

Fig. 1. Schematic diagram of loop thermosyphon.

2. Experimental prototype and procedures

2.1. Experimental setup

Schematic of the experimental setups for two loops are shown in Fig. 2. Each contained six major components: four cylindrical evaporators, a water tank, a condenser, two transport lines (vapor and liquid lines), a DC power supply, and a data acquisition system. Geometric specifications are given in Table 1. In one design (Fig. 2(a), 2(b)), the vapor head had U-symmetry; we refer to this design as top-U-symmetric. In the other design (Fig. 2(c), 2(d)), both vapor and liquid heads had U-symmetry; we call this both-U-symmetric. In both designs, four evaporators were placed below the condenser to obtain a return flow under gravity and the entire evaporators were well insulated with spongy thermal insulation. In this experiment, each evaporator was a grooved aluminum extrusion tube, as shown in Fig. 3(a). Although a real solar water heater uses radiant solar energy, it is difficult to consistently collect solar radiant energy in a test environment, which causes problems in calculating storage efficiency. Therefore, in our tests of the designs, we used a DC power supply, rather than solar energy, as the heat source. The heater used in these experiments was a copper plate inserted in a heat rod and placed on a flat surface of each evaporator, as shown in Fig. 3(b). The heat transfer area on the flat surface was 300 (L) mm × 15 (W) mm. To improve heat transfer efficiency, each cylindrical evaporator contained a porous wick material, and rectangular fins were attached to the wall of the wick. The porous wick was made of polyethylene and had an effective capillary radius of 9.34×10^{-5} m and a permeability of 6.84×10^{-13} m^2. We tested porous wicks with three different lengths inside the evaporator: 45, 15, and 0 cm. These are shown in Fig. 4. The condenser was a copper tube immersed in a 10 L tank; the tank also contained a submersible pump (flow: 300 L/h, power: 4.0 W, head: 0.6 m) at the bottom, as shown in Fig. 5. The pump ensured that the cooling water maintained a uniform temperature throughout the tank. The initial temperature of the cooling water was 22°C ± 1°C, and the volume of water in the tank was fixed at 9 L. Room temperature was maintained at 22°C ± 2°C through the use of an air conditioner.

The measurement system consisted of eleven T-type thermocouples installed on pipe walls at the locations shown in Fig. 2 and Fig. 3. All thermocouples were connected to a programmable controller to record temperature readings. Thermocouples T_{V1}, T_{V2}, T_{V3}, and T_{V4} were placed on the vapor outlets of evaporators I, II, III and IV, respectively. Thermocouples T_{L1}, T_{L2}, T_{L3}, and T_{L4} were placed on the liquid inlets of evaporators I, II, III, and IV, respectively. Thermocouple $T_{c,in}$

sampled the condenser inlet temperature, while thermocouples Tw,up and Tw,down measure water temperatures near the top and bottom of the water tank, respectively. The distance between thermocouples $T_{w,up}$ and $T_{w,down}$ was approximately 220 mm and the height of $T_{w,down}$ was 50 mm from the bottom of the tank. The working fluid was methanol. The charge ratio of the working fluid has a significant effect on start-up and operation of the loop. At low charge ratios, the wick dries out. At high charge ratios, the active condenser area becomes small and is not sufficient for heat removal [8]. Therefore, in the present experiments, the charge ratio of the working fluid was set to 50% for both loop designs. The vacuum before charging the working fluid was below 10^{-3} Pa. We started the experiments with a heating power of 120 W and increased it up to 360 W in increments of 80 W.

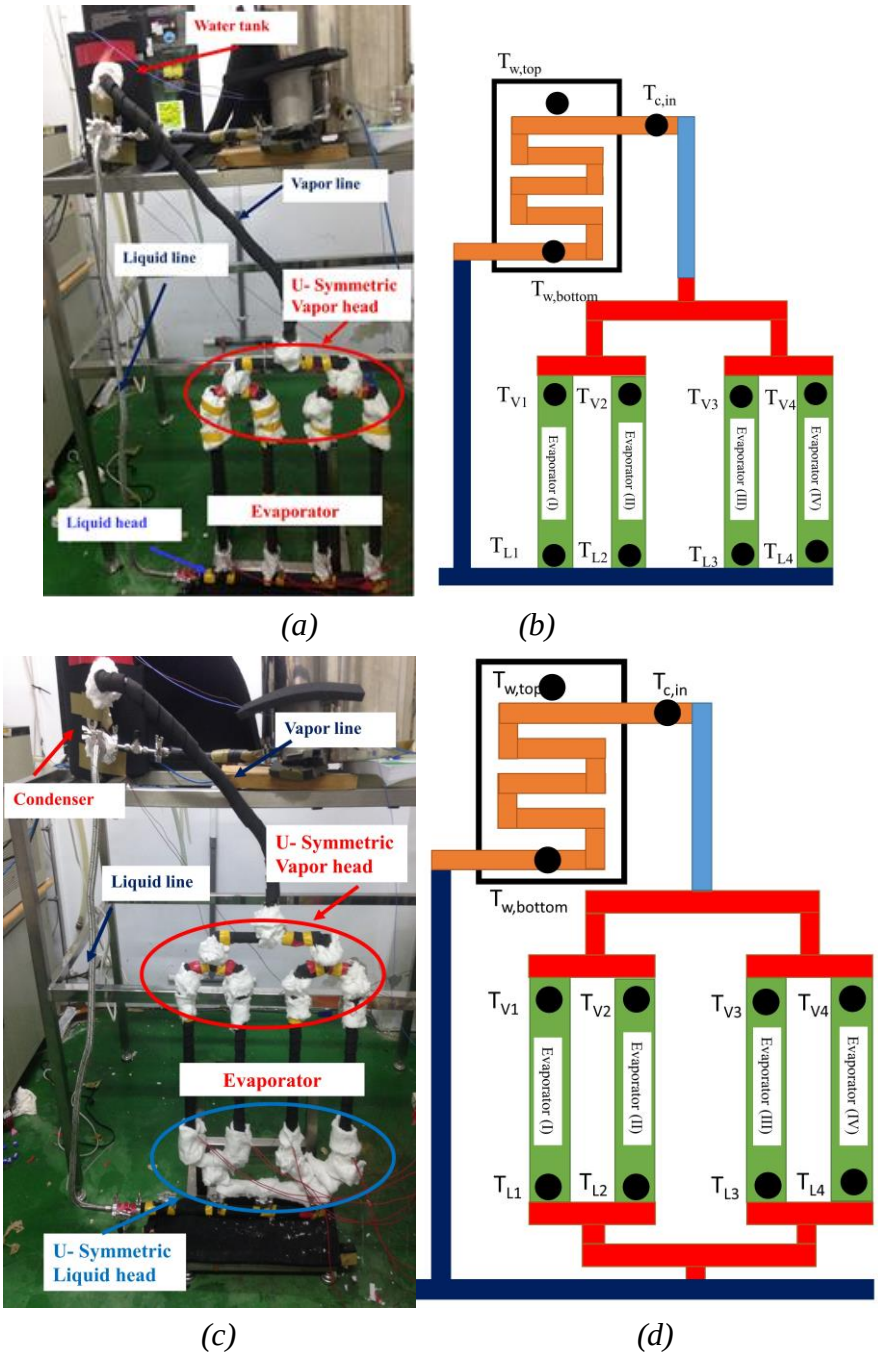

Fig. 2. The two loop thermosyphon solar thermal storage systems tested in this study. (a) Photograph of the system with the U-symmetric vapor head. (b) Schematic showing locations of thermocouples in the system in Panel (a). (c) Photograph of the system with U-symmetric vapor and liquid heads. (d) Schematic showing locations of thermocouples in the system in Panel (c).

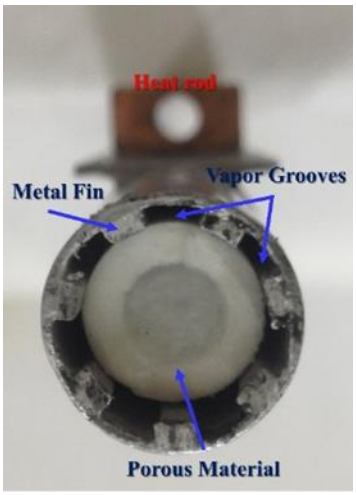

Fig. 3(a)

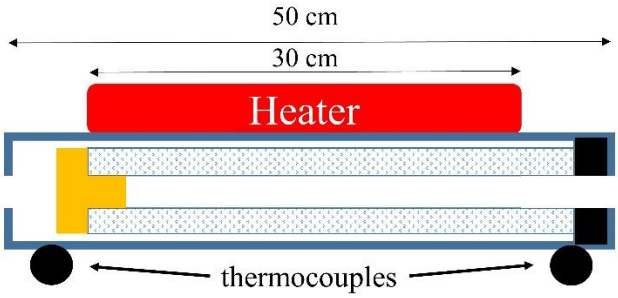

Fig. 3(b)

Fig. 3. Schematic of the evaporator. (a) Radial cross section of an evaporator tube. (b) Schematic showing locations of the thermocouples and heater in the evaporator tube.

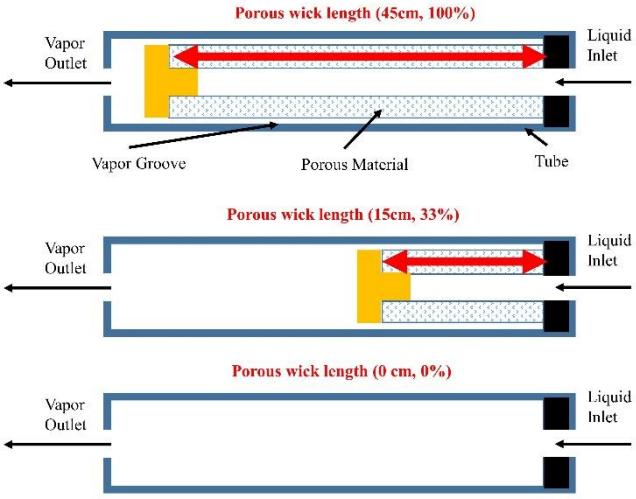

Fig. 4. Axial cross section of an evaporator tube containing porous wicks of three different lengths.

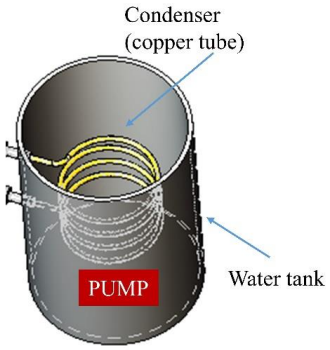

Fig. 5. Schematic of the condenser.

Table 1. Geometric specifications for components in the loop thermosyphon thermal storage system.

Element		*(mm)*
Evaporator	Outer diameter :	19
	Inner diameter :	12.5
	Length :	500
Condenser	Outer diameter :	6.35
	Inner diameter :	5.35
	Length :	1800
Water tank	Outer diameter :	21
	Inner diameter :	20
	Height :	320
Liquid Line	Outer diameter :	20.5
	Inner diameter :	18.5
	Length :	1500
Vapor Line	Outer diameter :	20.5
	Inner diameter :	18.5
	Length :	1000
Heater	Length :	300
	Width :	15
U symmetry structure	Outer diameter :	20.5
	Inner diameter :	18.5
	Total Length :	1300
Porous wick	Outer diameter :	12.5
	Inner diameter :	9.5

2.2. Data reduction and uncertainty analysis

The thermal storage efficiency (η_{th}) is the amount of thermal energy stored ($Q_{reservoir}$) in the water tank divided by the power provided to the system (Q_{in}) by the DC power supply [3],

$$\eta_{th} = Q_{reservoir} / Q_{in} \times 100, \quad (1)$$

$$Q_{reservoir} = mc_p \times (T_{w,t2} - T_{w,t1}), \quad (2)$$

$$T_w = (T_{w,top} + T_{w,bottom}) / 2, \quad (3)$$

$$Q_{in} = P_{total} \times (t_2 - t_1), \quad (4)$$

Here, m is the mass of water in the water tank, C_p is the heat capacity of water, P_{total} is the power supply output power, $T_{w,t1}$ and $T_{w,t2}$ are the average temperatures of water in the tank at the loop thermosyphon began operating time $_{t1}$ and final time $_{t2}$ of the experiment, respectively.

Temperatures provided by the thermocouples had uncertainties of ±1°C. An uncertainty analysis was performed according to [10]; the uncertainty in direct measurements is given as follows

$$e = \sqrt{e_s^{\,2} + e_r^{2}}\,, \qquad (5)$$

Here, e_s is the system uncertainty from the precision of instruments and e_r is the random uncertainty from the repeatability of measurements. Therefore, the maximum uncertainties for the charge ratio of the working fluid, DC power supply, and volume of water in the tank were ±5.38%, ±1.05%, and ±6.09%, respectively. Then, by the propagation of errors, the maximum uncertainty for thermal storage efficiency (η_{th}) was ±6.18%.

3. Results and discussion

3.1. Test results of two loop thermosyphon solar thermal storage systems

Figure 6 shows the start-up process of the top-U-symmetric design operating without a wick at two different values of input power: 120 W (30 W/evaporator) and 360 W (90 W/evaporator). In both cases, the temperatures at the evaporator liquid inlets were unstable; this was because the condensed working fluid to flow to each evaporator was not constant but random. However, the temperatures at each evaporator vapor outlet were very similar and stable with little increase. This was because the U-symmetry vapor head makes vapor bubbles flow uniformly from each evaporator. The increase in water temperature caused the temperature of condensed working fluid to increase, resulting in an increase in the evaporator outlet temperature over time. Figure 7 shows the temperature distribution of water in the tank. The temperatures at the top and bottom of the tank, $T_{w,top}$ and $T_{w,bottom}$, were nearly equal, indicating that the water temperature was nearly uniform everywhere in the water tank. However, Fig. 6 shows that the evaporator liquid inlet temperature was lower than the water temperature. This was because the liquid line was not thermally insulated; therefore, the working fluid released heat to the environment.

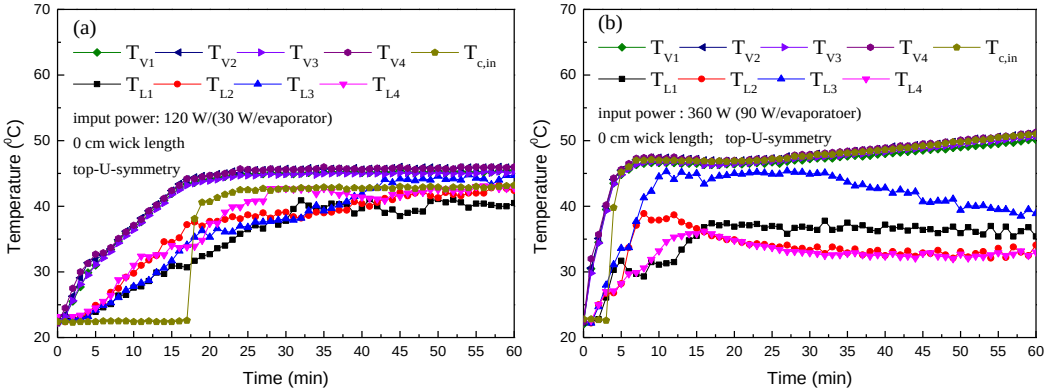

(a) *(b)*

Fig. 6. Temperature distributions in the evaporator in the top-U-symmetric design operating without a wick at two values of input power. (a) 120 W (30 W/evaporator) and (b) 360 W (90 W/evaporator).

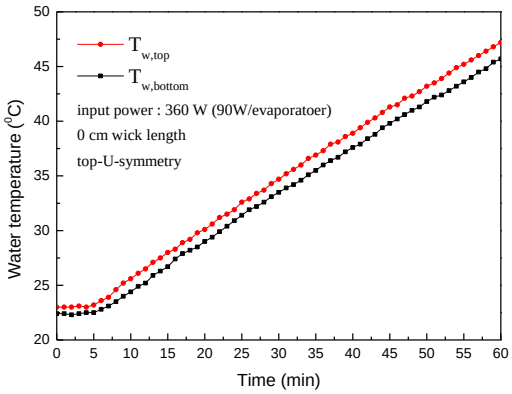

Fig. 7. Temperature distributions of water in the water tank.

To suppress the fluctuations in evaporator inlet temperature, the liquid head was changed to the U-symmetric design in Fig. 2(c). Then, both the vapor and liquid heads had U-symmetry. Figure 8 shows the start-up processes for two values of input power: 120 W (30 W/evaporator) and 360 W (90 W/evaporator). Now the temperature distributions at the liquid inlet were more stable than those in Fig. 6, and the temperature difference between the vapor outlet and liquid inlet became much higher than those in the loop that had U-symmetry only at the vapor head. The U-symmetry of the liquid head caused the condensed working fluid to flow to each evaporator in a stable manner, causing the temperature distributions at the liquid inlet to be more stable. Consequently, a loop with a top-U-symmetric head would have decreased thermal storage efficiencies, as shown in Fig. 9. The thermal storage efficiency increased as the heating power increased from 120 W to 360 W. When heating power was low, the frequency of generation of vapor bubbles in the evaporator was low, leading to low values for heat transfer coefficients. As heating power was increased, nucleate boiling increased, resulting in higher heat transfer coefficients, so thermal storage efficiency increased.

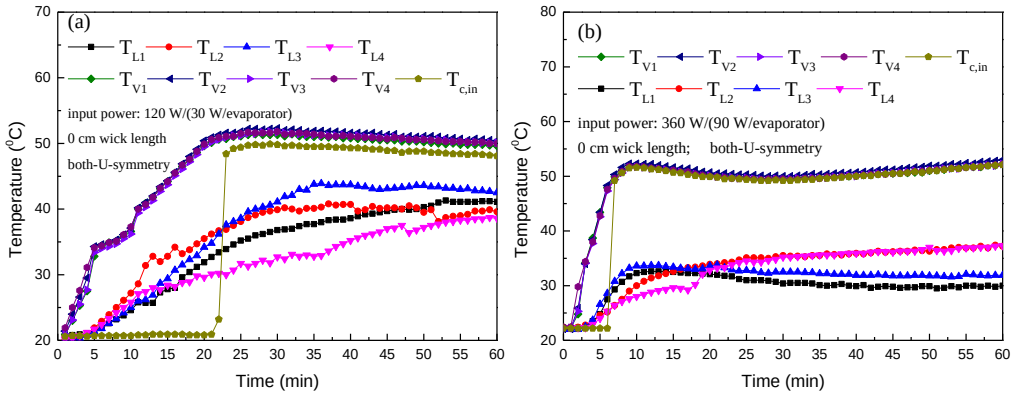

(a) *(b)*

Fig. 8. Temperature distributions in evaporators for the both-U-symmetric design operating without a wick at two values of input power. (a) 120 W (30 W/evaporator), (b) 360 W (90 W/evaporator). The symbols are defined in the caption to Fig. 6.

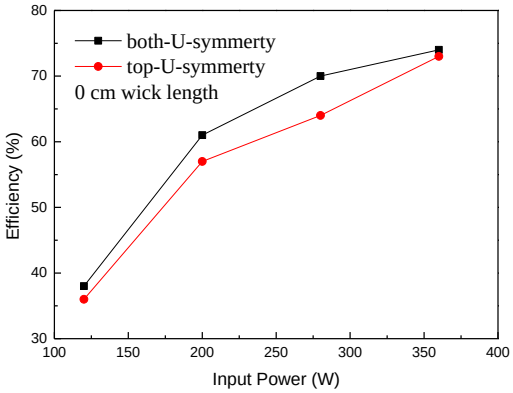

Fig. 9. Comparison of thermal storage efficiencies for top-U- and both-U-symmetric designs operating without wicks at selected values of input power.

3.2. Porous wick effect

To improve thermal storage efficiency, a porous wick was installed inside each evaporator, as in Fig. 4. The porous wick in the evaporator serves several functions [11]: (a) it absorbs working fluid when vaporization occurs, (b) it prevents flow of vapor into the liquid inlet, and (c) it reduces heat leaks from the evaporator to the liquid inlet. However, a porous wick has large thermal resistance and increases the frictional resistance to working fluid [12]. Although both-U-symmetry has highly thermal storage efficiencies, its structure is more complex. The solar water heater usually use simple structure. In addition, the efficiency of both-U-symmetry is a little higher than top-U-symmetry. Therefore, use the top-U-symmetry to study porous wick effect.

Figure 10 shows the start-up process using porous wicks with lengths of 45 cm and 15 cm at two different values of input power. With the porous wick inside the evaporator, the liquid inlet temperature decreased compared to those with no porous wick at low input power. These differences were because the porous wick increased the evaporator thermal resistance and reduced heat leaks to the liquid head.

The above results are for start-up of the loop thermosyphon at low input power. However, at high input power and after 60 min, the evaporator vapor outlet temperature was about 50°C for all three porous wick lengths, indicating that the effects of the porous wick decreased as the input power increased. Figure 11 shows the thermal storage efficiencies for the three different lengths of porous wick. The thermal storage efficiency increased with increasing wick length, especially at low input power. This was because increases in wick length reduced heat leaks to the liquid head. This led to more heat being applied in the evaporator and more heat transfer in the condenser, so efficiency improved.

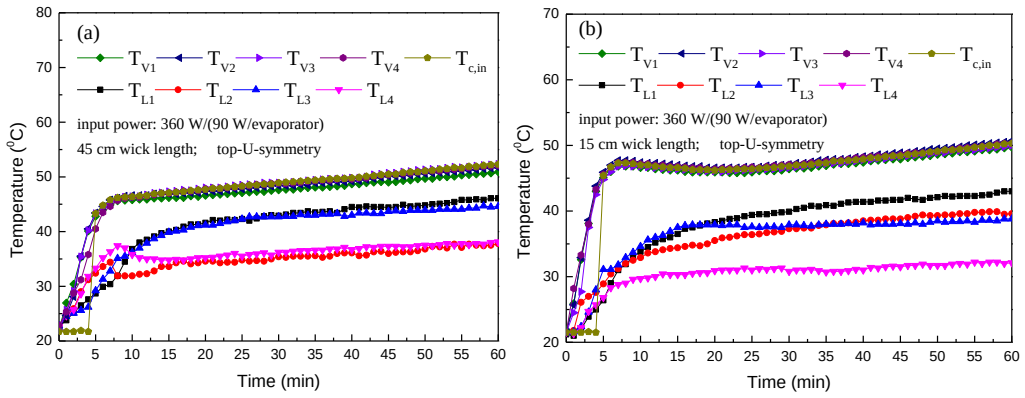

(a) *(b)*

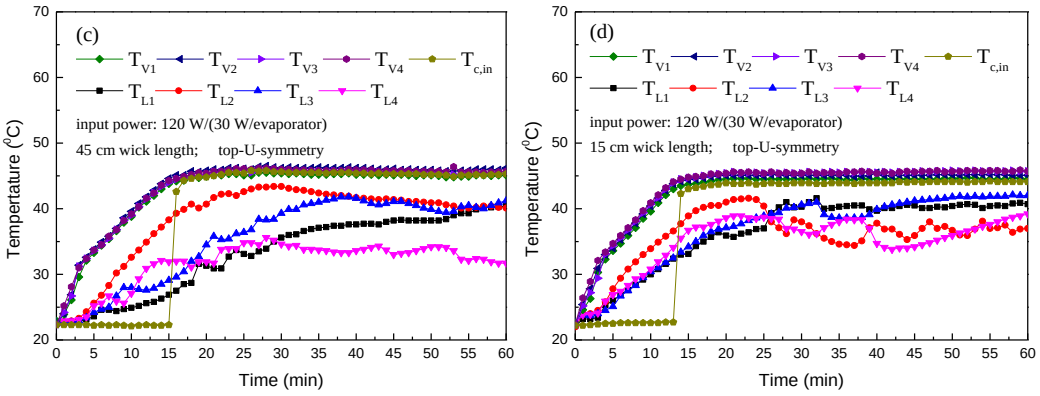

(c) *(d)*

Fig. 10. Temperature distributions in evaporators for top-U-designs at different values of input power and different lengths of porous wick. (a) 360 W (90 W/evaporator), 45-cm wick, (b) 360 W (90 W/evaporator), 15-cm wick, (c) 120 W (30 W/evaporator), 45-cm wick, (c) 120 W (30 W/evaporator), 15-cm wick. The symbols are defined in the caption to Fig. 6.

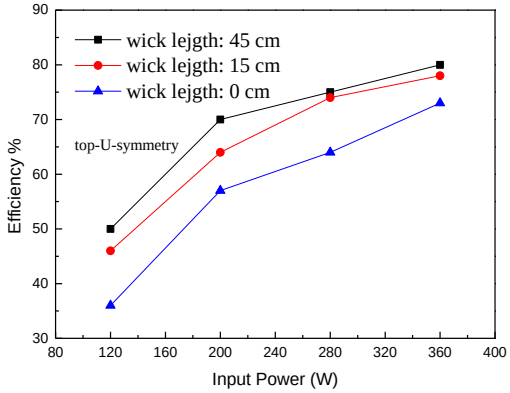

Fig. 11. Thermal storage efficiencies of the top-U-symmetric design at different wick lengths.

The above results all show the same behavior of vapor outlet temperature: all evaporator vapor outlet temperatures were the same and stable, although evaporator liquid inlet temperatures were very unstable. This may have been due to sharing of heat load among evaporators. Therefore, the uneven heat loads applied to each evaporator were tested. Figure 12 shows temperature distributions when a heating power of 90 W was provided only to one evaporator (I). As heat was applied to evaporator I, the vapor and liquid head temperatures T_{V1} and T_{L1} rose immediately and reached steady state. Simultaneously, the head temperatures of the other evaporators remained almost at ambient. After some minutes, the temperatures on evaporator II, T_{V2} and T_{L2}, also increased. This was because vapor generated in evaporator I flowed, not only to the condenser, but also into evaporator II through the U-symmetric vapor head, causing all evaporator vapor outlets to reach similar temperatures.

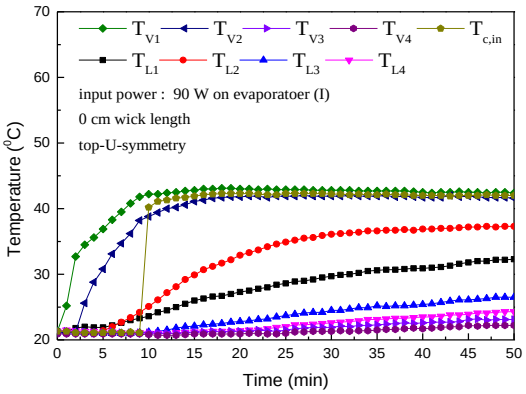

Fig. 12. Temperature distributions in evaporators when heat was applied only to evaporator (I). The symbols are defined in the caption to Fig. 6.

3. Conclusions

In this study, we experimentally investigated a loop thermosyphon with four evaporators for use as a solar water heater. The thermal storage efficiency of the loop thermosyphon solar water heater was analyzed in detail, and the following conclusion can be drawn.

1. A U-symmetric vapor head made the vapor flow uniformly from each evaporator, causing all four evaporators to have the same temperature at their vapor outlets.
2. A U-symmetric liquid head caused the condensed working fluid to flow to each evaporator in a stable manner, causing the evaporators to have a more stable temperature distribution at their liquid inlets. Therefore, the both-U-symmetric would have higher thermal storage efficiencies than top-U-symmetric.
3. With a porous wick inside the evaporator, the loop had a higher thermal storage efficiency, especially at low input power. The wick reduced heat leaks to the liquid head, and as a result, the wick was helpful during start-up.
4. Sharing of heat load was observed when input power was applied to just one evaporator (I). Heat from evaporator (I) flowed not only to the condenser but also into evaporator (II). This demonstrates that some of the heat applied to evaporator (I) was actually used to warm evaporator (II).
5. The highest thermal storage efficiency obtained in our experiments was 80 ± 6.18%, for a top-U-symmetric installed with a 45 cm wick.

Acknowledgments

This project is supported by National Science Council, Taiwan, NSC-103-2623-E-007-008- ET. We acknowledge NSC for their support for this project.

Nomenclature

c_p specific heat, J/(kg K)

T temperature, °C

m water quantity in the storage tank, g

Q energy, J

P_{total} the power supply output power, W

Greek symbols

η_{th} efficiency

Subscripts and superscripts

w water

t1 the loop thermosyphon began operating time

t2 the loop thermosyphon final time of the experiment

References

[1] Husseina H.M.S., Mohamada M.A., El-Asfourib A.S., Transient investigation of a thermosyphon flat-plate solar collector, Appl. Therm. Eng. 19 (1999) 789–800.

[2] Wang Z., Yang W., Qiu F., Zhang X., Zhao X., Solar water heating: From theory, application, marketing and research, Renew. Sust. Energ. Rev. 41 (2015) 68–84.

[3] Chien C.C., Kungb C.K., Changb C.C., Leea W.S., Jwoa C.S., Chenb S.L., Theoretical and experimental investigations of a two-phase thermosyphon solar water heater, Energy 36 (2011) 415–423.

[4] Lu L., Liu Z.H., Xiao H.S., Thermal performance of an open thermosyphon using nanofluids for high-temperature evacuated tubular solar collectors Part 1: Indoor experiment, Sol. Energy 85 (2011) 379–387.

[5] Zhang X., Zhao X., Xu J., Yu X., Characterization of a solar photovoltaic/loop-heat-pipe heat pump water heating system, Appl. Energy 102 (2013)1229–1245.

[6] Zhang X., Zhao X., Shen J., Hu X., Liu X., Xu J., Design, fabrication and experimental study of a solar photovoltaic/loop-heat-pipe based heat pump system, Sol. Energy 97 (2013) 551–568.

[7] Lia J., Linb F., Niub G., An insert-type two-phase closed loop thermosyphon for split-type solar water heaters, Appl. Therm. Eng. 70 (2014) 441–450.

[8] Chen B.B., Liu W., Liu Z.C., Li H., Yang J.G., Experimental investigation of loop heat pipe with flat evaporator using biporous wick, Appl. Therm. Eng. 42 (2012) 34–40.

[9] Ku J., Operating Characteristics of Loop Heat Pipes, 29th International Conference on Environmental System, 1999

[10] Moffat R.J., Describing the uncertainties in experimental results, Exp. Therm. Fluid Sci. 1 (1988) 3–17.

[11] Chen P.C., Lin W.K., The application of capillary pumped loop for cooling of electronic components, Appl. Therm. Eng. 21 (2001) 1739–1754.

[12] Wang S., Zhang W., Zhang X., Chen J., Study on start-up characteristics of loop heat pipe under low-power, Int. J. Heat. Mass. Tran. 54 (2011) 1002–1007.